

Precision bounds for quantum phase estimation using two-mode squeezed Gaussian states

Jian-Dong Zhang(张建东), Chuang Li(李闯), Lili Hou(侯丽丽), and Shuai Wang(王帅)

Citation: Chin. Phys. B, 2025, 34 (**1**): 010304. DOI: 10.1088/1674-1056/ad8dc0
Journal homepage: http://cpb.iphy.ac.cn; http://iopscience.iop.org/cpb

What follows is a list of articles you may be interested in

Generation of broadband polarization-orthogonal photon pairs via the dispersion-engineered thin-film lithium niobate waveguide

Ji-Ning Zhang(张继宁), Tong-Yu Zhang(张同宇), Jia-Chen Duan(端家晨), Yan-Xiao Gong(龚彦晓), and Shi-Ning Zhu(祝世宁)
Chin. Phys. B, 2024, 33 (**11**): 110301. DOI: 10.1088/1674-1056/ad757c

Micron-sized fiber diamond probe for quantum precision measurement of microwave magnetic field

Wen-Tao Lu(卢文韬), Sheng-Kai Xia(夏圣开), Ai-Qing Chen(陈爱庆), Kang-Hao He(何康浩), Zeng-Bo Xu(许增博), Yi-Han Chen(陈艺涵), Yang Wang(汪洋), Shi-Yu Ge(葛仕宇), Si-Han An(安思瀚), Jian-Fei Wu(吴建飞), Yi-Han Ma(马艺菡), and Guan-Xiang Du(杜关祥)
Chin. Phys. B, 2024, 33 (**8**): 080305. DOI: 10.1088/1674-1056/ad5321

Enhancing quantum metrology for multiple frequencies of oscillating magnetic fields by quantum control

Xin Lei(雷昕), Jingyi Fan(范静怡), and Shengshi Pang(庞盛世)
Chin. Phys. B, 2024, 33 (**6**): 060304. DOI: 10.1088/1674-1056/ad3430

Holevo bound independent of weight matrices for estimating two parameters of a qubit

Chang Niu(牛畅) and Sixia Yu(郁司夏)
Chin. Phys. B, 2024, 33 (**2**): 020304. DOI: 10.1088/1674-1056/ad117d

Tolerance-enhanced SU(1,1) interferometers using asymmetric gain

Jian-Dong Zhang(张建东) and Shuai Wang(王帅)
Chin. Phys. B, 2023, 32 (**1**): 010306. DOI: 10.1088/1674-1056/ac981d

---

Precision bounds for quantum phase estimation using two-mode squeezed Gaussian states

Jian-Dong Zhang(张建东)[1,†], Chuang Li(李闯)[2], Lili Hou(侯丽丽)[1], and Shuai Wang(王帅)[1]

[1] *School of Mathematics and Physics, Jiangsu University of Technology, Changzhou* 213001, *China*
[2] *Research Center for Novel Computing Sensing and Intelligent Processing, Zhejiang Laboratory, Hangzhou* 311121, *China*

(Received 2 September 2024; revised manuscript received 22 October 2024; accepted manuscript online 1 November 2024)

Quantum phase estimation based on Gaussian states plays a crucial role in many application fields. In this paper, we study the precision bound for the scheme using two-mode squeezed Gaussian states. The quantum Fisher information is calculated and its maximization is used to determine the optimal parameters. We find that two single-mode squeezed vacuum states are the optimal Gaussian inputs for a fixed two-mode squeezing process. The corresponding precision bound is sub-Heisenberg-limited and scales as $N^{-1}/2$. For practical purposes, we consider the effects originating from photon loss. The precision bound can still outperform the shot-noise limit when the lossy rate is below 0.4. Our work may demonstrate a significant and promising step towards practical quantum metrology.

Keywords: quantum metrology, Gaussian state, Heisenberg limit

PACS: 03.67.–a, 42.50.–p, 42.50.Dv

DOI: 10.1088/1674-1056/ad8dc0 **CSTR:** 32038.14.CPB.ad8dc0

1. Introduction

Phase estimation based on optical interferometers is a fundamental means to achieve high-precision measurements for many important physical quantities, concentration, magnetic fields, gravitational waves, to name a few. Quantum phase estimation can provide enhanced precision beyond the shot-noise limit, which is the precision bound attainable by exploiting classical resources. In this regard, the quantum Fisher information (QFI) is an effective tool to evaluate the precision bound for a specific input and parameterization.[1,2] To be specific, the precision bound is equal to the reciprocal of square root of the QFI. Related to this, the QFIs corresponding to the shot-noise limit and the Heisenberg limit scale as N and N^2, where N is the total average photon number employed for phase estimation. It is particularly important for single-phase estimation, since the precision bound given by the QFI can always be asymptotically saturated through specific positive-operator-valued measure (POVM) and maximum likelihood estimation.

In terms of the parameter estimation theory, any interferometer can be divided into three parts including probe preparation, phase encoding, and POVM. The precision bound is completely determined by the first two parts. In general, the part of phase encoding is deterministic; therefore, improving the precision bound requires the engineering of the probe preparation. Related to this, two methods are usually deployed. The first method utilizes a linear beam splitter to combine two single-mode inputs, while the two inputs in the second method are combined by a nonlinear beam splitter, i.e., optical parametric amplifier (OPA). The interferometers with these two methods are known as linear and nonlinear interferometers, respectively.

Over the past decades, numerous efforts have been made in quantum phase estimation based on linear interferometers. Many exotic quantum states were considered as the input, such as single/two-mode squeezed vacuum states,[3–6] N00N states,[7,8] entangled coherent states,[9,10] and coherent along with squeezed states.[11–13] The precision bounds for the schemes using these above states can outperform the shot-noise limit and reach the Heisenberg limit. In recent years, quantum phase estimation using nonlinear interferometers has also received lots of attention.[14–24] In this configuration, two inputs undergo a two-mode squeezing process provided by the first OPA. The correlation between the two modes is improved, and the total average number of photons is also increased. These two types of interferometers have their own advantages. As a result, quantum phase estimation using hybrid or nested interferometers composed of nonlinear and linear beam splitters has also drawn considerable interest.[25–29]

The aforementioned studies analyzed the precision bounds for the schemes using some specific inputs. Recently, exploring the optimal inputs by maximizing the QFI has been reported in a linear interferometer. Lang *et al.* analyzed the optimal input for the second port with the first port fed by a coherent state.[30] Zhang *et al.* discussed the optimal single-mode input.[31] The optimal separable Gaussian inputs were showed by Sparaciari *et al.*[32] In this paper, we extend the problem of determining the optimal inputs to nonlinear inter-

[†]Corresponding author. E-mail: zhangjiandong@jsut.edu.cn

© 2025 Chinese Physical Society and IOP Publishing Ltd. All rights, including for text and data mining, AI training, and similar technologies, are reserved.

ferometers. We consider two general single-mode Gaussian states as the inputs. The precision bound given by the QFI is calculated and maximized by selecting the best parameters. We analyze the precision bound in a lossy environment and discuss the tolerance against photon loss. This work may provide a positive complement to the aspect of quantum phase estimation using nonlinear interferometers and relevant variants.

The remainder of this paper is organized as follows. Section 2 introduces the estimation scheme and provides the general expression for the QFI. Section 3 determines the optimal inputs by maximizing the QFI, and the corresponding precision bound is analyzed. In Section 4, we study the precision bound in the presence of photon loss and compare it with the precision bound of a classical-quantum hybrid scheme. Finally, we summarize main results in Section 5.

2. Estimation scheme and quantum Fisher information

Figure 1 gives the schematic diagram of quantum phase estimation using two-mode squeezed Gaussian states. Two single-mode Gaussian states pass through an OPA and evolve into two-mode squeezed Gaussian states. The estimated phase φ is encoded into the state in mode a, and a POVM is performed.

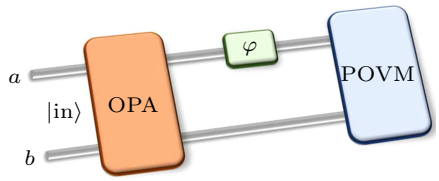


Fig. 1. Schematic diagram of quantum phase estimation using two-mode squeezed Gaussian states. OPA: optical parametric amplifier, POVM: positive-operator-valued measure.

Since the two-mode squeezing process implemented by the OPA is fixed, the task in this paper is to find the optimal Gaussian inputs. The most general single-mode Gaussian states can be expressed as displaced squeezed thermal states.[33] Meanwhile, for phase estimation, it is no use to prepare thermal states as the inputs.[34] As a consequence, we only need to consider pure Gaussian inputs, two single-mode displaced squeezed vacuum states. Without loss of generality, we assume that two states in modes a and b are the same. Specifically, the input can be written as

$$|\text{in}\rangle = \hat{D}(\alpha)\hat{S}(\xi)|0\rangle \otimes \hat{D}(\alpha)\hat{S}(\xi)|0\rangle, \tag{1}$$

where $\hat{D}(\alpha)$ is the displacement operator with $\alpha = |\alpha|\,\mathrm{e}^{\mathrm{i}\delta}$ being the displacement amplitude, $\hat{S}(\xi)$ is the squeezing operator with $\xi = r\mathrm{e}^{\mathrm{i}\theta}$ being the squeezing parameter. Further, the average photon number of the inputs is given by

$$N_{\text{in}} = \langle \text{in}|(\hat{a}^\dagger\hat{a} + \hat{b}^\dagger\hat{b})|\text{in}\rangle = 2(|\alpha|^2 + \sinh^2 r), \tag{2}$$

where $\hat{a}^\dagger$ ($\hat{b}^\dagger$) and $\hat{a}$ ($\hat{b}$) are creation and annihilation operators for mode a (b). The relation between the mode operators and displacement operator is

$$\hat{D}^\dagger(\alpha)\hat{a}\hat{D}(\alpha) = \hat{a} + \alpha, \tag{3}$$

$$\hat{D}^\dagger(\alpha)\hat{b}\hat{D}(\alpha) = \hat{b} + \alpha, \tag{4}$$

and the relation between the mode operators and single-mode squeezing operator is

$$\hat{S}^\dagger(\xi)\hat{a}\hat{S}(\xi) = \hat{a}\cosh r - \mathrm{e}^{\mathrm{i}\theta}\hat{a}^\dagger \sinh r, \tag{5}$$

$$\hat{S}^\dagger(\xi)\hat{b}\hat{S}(\xi) = \hat{b}\cosh r - \mathrm{e}^{\mathrm{i}\theta}\hat{b}^\dagger \sinh r. \tag{6}$$

Due to the gain of the two-mode squeezing process, photons are increased after the OPA. The total average number of photons in our scheme is found to be

$$\begin{aligned} N &= \langle \text{in}|\hat{S}^\dagger_{\text{OPA}}(g)(\hat{a}^\dagger\hat{a} + \hat{b}^\dagger\hat{b})\hat{S}_{\text{OPA}}(g)|\text{in}\rangle \\ &= N_{\text{in}}\cosh 2g + 2|\alpha|^2\cos(2\delta - \phi)\sinh 2g + 2\sinh^2 g, \end{aligned} \tag{7}$$

where we used the following relation:

$$\hat{S}^\dagger_{\text{OPA}}(g)\hat{a}\hat{S}_{\text{OPA}}(g) = \hat{a}\cosh g + \mathrm{e}^{\mathrm{i}\phi}\hat{b}^\dagger \sinh g, \tag{8}$$

$$\hat{S}^\dagger_{\text{OPA}}(g)\hat{b}\hat{S}_{\text{OPA}}(g) = \hat{b}\cosh g + \mathrm{e}^{\mathrm{i}\phi}\hat{a}^\dagger \sinh g \tag{9}$$

with $S_{\text{OPA}}(g)$ being the two-mode squeezing operator, g and ϕ being the strength and phase of the gain.

Now we analyze the precision bound of our scheme. Since the inputs and operations are Gaussian, all information regarding the estimated phase can be obtained via the mean vector and variance matrix of the outputs. For this reason, we calculate the QFI through the use of symplectic geometry method.[33,35] Let us consider the vector composed of quadrature operators of modes a and b

$$\hat{\boldsymbol{X}} = [\,\hat{a}^\dagger + \hat{a} \;\; \mathrm{i}(\hat{a}^\dagger - \hat{a}) \;\; \hat{b}^\dagger + \hat{b} \;\; \mathrm{i}(\hat{b}^\dagger - \hat{b})\,]^{\mathrm{T}}. \tag{10}$$

For the inputs in Eq. (1), the mean vector is given by

$$\boldsymbol{M}_{\text{in}} = \langle \hat{\boldsymbol{X}} \rangle = 2|\alpha| \cdot [\,\cos\delta \;\; \sin\delta \;\; \cos\delta \;\; \sin\delta\,]^{\mathrm{T}} \tag{11}$$

and the covariance matrix is given by

$$\boldsymbol{\Sigma}_{\text{in}} = \begin{bmatrix} \mathrm{e}^{2r} & 0 & 0 & 0 \\ 0 & \mathrm{e}^{-2r} & 0 & 0 \\ 0 & 0 & \mathrm{e}^{2r} & 0 \\ 0 & 0 & 0 & \mathrm{e}^{-2r} \end{bmatrix}, \tag{12}$$

whose arbitrary matrix element is defined by

$$\boldsymbol{\Sigma}_{kn} = \frac{1}{2}\langle \hat{\boldsymbol{X}}_k\hat{\boldsymbol{X}}_n + \hat{\boldsymbol{X}}_n\hat{\boldsymbol{X}}_k\rangle - \langle \hat{\boldsymbol{X}}_k\rangle\langle \hat{\boldsymbol{X}}_n\rangle. \tag{13}$$

All expectation values $\langle\cdot\rangle$ in Eqs. (11) and (13) are taken over by the inputs. Based on the relations between optical operations and quadrature operators, we can write the transformation matrix for OPA (see Appendix for details)

$$\boldsymbol{U}_{\text{OPA}} = \begin{bmatrix} \cosh g & 0 & \sinh gC_\phi & \sinh gS_\phi \\ 0 & \cosh g & \sinh gS_\phi & -\sinh gC_\phi \\ \sinh gC_\phi & \sinh gS_\phi & \cosh g & 0 \\ \sinh gS_\phi & -\sinh gC_\phi & 0 & \cosh g \end{bmatrix} \tag{14}$$

and that for phase encoding

$$\boldsymbol{U}_{\rm PE}=\begin{bmatrix}\cos\varphi & -\sin\varphi & 0 & 0\\ \sin\varphi & \cos\varphi & 0 & 0\\ 0 & 0 & 1 & 0\\ 0 & 0 & 0 & 1\end{bmatrix} \tag{15}$$

with abbreviations $C_\phi\equiv\cos\phi$ and $S_\phi\equiv\sin\phi$. By using the transformation

$$\boldsymbol{M}_\varphi=\boldsymbol{U}_{\rm PE}\boldsymbol{U}_{\rm OPA}\boldsymbol{M}_{\rm in}, \tag{16}$$

we get the mean vector of the outputs after passing through the estimated phase. Similarly, the covariance matrix of the outputs can be obtained through the following transformation:

$$\boldsymbol{\Sigma}_\varphi=\boldsymbol{U}_{\rm PE}\boldsymbol{U}_{\rm OPA}\Sigma_{\rm in}\boldsymbol{U}_{\rm OPA}^{\rm T}\boldsymbol{U}_{\rm PE}^{\rm T}. \tag{17}$$

On the basis of the above results, the QFI turns out to be[35,36]

$$\mathcal{F}=\frac{1}{2}{\rm Tr}\left\{\partial_\varphi\boldsymbol{\Sigma}\left[\boldsymbol{\Sigma}\left(\partial_\varphi\boldsymbol{\Sigma}\right)^{-1}\boldsymbol{\Sigma}^{\rm T}+\frac{1}{4}\boldsymbol{\Omega}\left(\partial_\varphi\boldsymbol{\Sigma}\right)^{-1}\boldsymbol{\Omega}^{\rm T}\right]^{-1}\right\}+\left(\partial_\varphi\boldsymbol{M}\right)^{\rm T}\boldsymbol{\Sigma}^{-1}\left(\partial_\varphi\boldsymbol{M}\right), \tag{18}$$

where

$$\boldsymbol{M}=\boldsymbol{H}\boldsymbol{M}_\varphi, \tag{19}$$

$$\boldsymbol{\Sigma}=\boldsymbol{H}\boldsymbol{\Sigma}_\varphi\boldsymbol{H}^{\rm T}, \tag{20}$$

$\partial_\varphi\boldsymbol{M}=\partial\boldsymbol{M}/\partial\varphi$ and $\partial_\varphi\boldsymbol{\Sigma}=\partial\boldsymbol{\Sigma}/\partial\varphi$. The specific forms of two transformation matrices in Eq. (18) are given by

$$\boldsymbol{\Omega}=\begin{bmatrix}0 & 1 & 0 & 0\\ -1 & 0 & 0 & 0\\ 0 & 0 & 0 & 1\\ 0 & 0 & -1 & 0\end{bmatrix}, \tag{21}$$

$$\boldsymbol{H}=\frac{1}{2}\begin{bmatrix}1 & {\rm i} & 0 & 0\\ 1 & -{\rm i} & 0 & 0\\ 0 & 0 & 1 & {\rm i}\\ 0 & 0 & 1 & -{\rm i}\end{bmatrix}. \tag{22}$$

After straightforward calculation, we finally get the general expression for the QFI of our scheme

$$\mathcal{F}=\frac{\Delta}{8\,{\rm e}^{4r}} \tag{23}$$

with

$$\begin{aligned}\Delta\ =\ & {\rm e}^{4r}[8|\alpha|^2(2\cosh 2r+3\cos 2\delta\sinh 2r)+5\cosh 4r]\\ & +{\rm e}^{4r}[\cosh 4g(16|\alpha|^2\cosh 2r+3\cosh 4r+1)-9]\\ & +4|\alpha|^2({\rm e}^{6r}-{\rm e}^{2r})\left[2\cos(2\delta-2\phi)\sinh^2 2g\right.\\ & \left.+\cosh 4g\cosh 2{\rm i}\phi\right]+({\rm e}^{4r}-1)^2\cos 2\phi\sinh^2 2g-1\\ & +16|\alpha|^2{\rm e}^{2r}\sinh 4g\left[{\rm e}^{4r}\cos\delta\cos(\delta-\phi)\right.\\ & \left.-\sin\delta\sin(\delta-\phi)\right].\end{aligned} \tag{24}$$

One can find that both the QFI and total average photon number reach the maximal values with the optimal phase-matching condition $\delta=\phi=0$. At this point, we have

$$N=2|\alpha|^2{\rm e}^{2g}+2\sinh^2 r\cosh 2g+2\sinh^2 g, \tag{25}$$

$$\mathcal{F}=2|\alpha|^2{\rm e}^{2r}(1+{\rm e}^{4g})+\cosh 4r\cosh^2 2g-1, \tag{26}$$

which are used in the following analysis.

3. Optimal inputs and precision bound

Given the current experimental techniques,[37] we can reasonably assume $|\alpha|^2\gg 1$ and utilize the following abbreviations:

$$G\equiv\sinh^2 g\approx\cosh^2 g\approx\frac{{\rm e}^{2g}}{4}, \tag{27}$$

and define the ratio of displacement portion to squeezing portion in the inputs as k ($k\geq 0$), i.e.,

$$k\equiv\frac{|\alpha|^2}{\sinh^2 r}. \tag{28}$$

Related to this, the total average photon number in Eq. (25) can be approximately expressed as

$$N\approx(8k+4)\sinh^2 rG \tag{29}$$

and the QFI can be approximately written as

$$\mathcal{F}\approx(32k{\rm e}^{2r}\sinh^2 r+4\cosh 4r)G^2. \tag{30}$$

Based on these results, we have

$$\frac{\mathcal{F}}{N^2}\approx\frac{2k}{4k^2+4k+1}\frac{{\rm e}^{2r}}{\sinh^2 r}+\frac{1}{4k^2+4k+1}\frac{\cosh 4r}{4\sinh^4 r}. \tag{31}$$

It is not difficult to find that the maximal value is obtained if the condition $k=0$ is satisfied. Hence, $k=0$ is the optimal ratio for maximizing the QFI, and the optimal inputs are two single-mode squeezed vacuum states. Related to this, the average photon number of the inputs is reduced to $N_{\rm in}=2\sinh^2 r$ and the total average photon number becomes

$$N=2\sinh^2 r\cosh 2g+2\sinh^2 g. \tag{32}$$

The corresponding QFI arrives

$$\mathcal{F}_{S\otimes S}=\cosh 4r\cosh^2 2g-1. \tag{33}$$

In the case of $\sinh^2 g\gg 1$, one can get

$$\mathcal{F}_{S\otimes S}\approx 2N^2 \tag{34}$$

with the increase of r. Even if the value of r is small, the precision bound is superior to the Heisenberg limit, i.e., $\mathcal{F}_{S\otimes S}>N^2$. In this regard, a well-known example is $r=0$ (two vacuum states), which also shows sub-Heisenberg-limited precision bound.[38]

Since two single-mode squeezed vacuum states are used as the inputs, our scheme is a pure quantum scheme. In a lossless environment, it is superior to a pure classical scheme using two coherent states as inputs ($\mathcal{F}\approx 4N^2/3$);[39] meanwhile, it surpasses a classical-quantum hybrid scheme using coherent along with squeezed vacuum states as inputs ($\mathcal{F}\approx 3N^2/2$).[35]

4. Precision bound in the presence of photon loss

For any optical system, photon loss is always inevitable and is main hindrance to achieve high precision. This process can be simulated by adding fictitious beam splitters. The reflection of the fictitious beam splitter leads to a decrease in the number of photons; meanwhile, the coupling of vacuum fluctuation reduces the coherence of quantum states. Both of these two factors result in a degradation of the precision. For practical purposes, in this section we analyze the precision bound of our scheme in a lossy environment.

Generally, a quantum state after a lossy process becomes a mixed state. At this point, it is quite difficult to give an analytical expression for the QFI. In particular, for Gaussian states, symplectic geometry method can provide an analytical result. Let us use L to represent the lossy rate. Then the mean vector and covariance matrix in a lossy environment can be written as[40,41]

$$\boldsymbol{M}_{\varphi} = \sqrt{1-L}\cdot\boldsymbol{U}_{\rm PE}\boldsymbol{U}_{\rm OPA}\boldsymbol{M}_{\rm in}, \tag{35}$$

$$\boldsymbol{\Sigma}_{\varphi} = (1-L)\boldsymbol{U}_{\rm PE}\boldsymbol{U}_{\rm OPA}\boldsymbol{\Sigma}_{\rm in}\boldsymbol{U}_{\rm OPA}^{\rm T}\boldsymbol{U}_{\rm PE}^{\rm T} + L\boldsymbol{I}_4, \tag{36}$$

where $\boldsymbol{I}_4$ is four-by-four identity matrix. The above results suggest that a quantum state after photon loss becomes a statistical mixture of the attenuated quantum state and a vacuum state.

By substituting Eqs. (35) and (36) into Eq. (18), the QFI in a lossy environment is found to be

$$\mathcal{F}_{S\otimes S}^{\rm L} = \frac{(1-L)^2\Delta_1}{4\Delta_2} \tag{37}$$

with

$$\begin{aligned}
\Delta_1 =\ & 4(L-L^2)\,{\rm e}^{4r}\cosh 2r\cosh 2g\,[\cosh 4g + 2\cosh 4r - 3] \\
& + (1+{\rm e}^{8r})(2-2L+L^2) \\
& + 2{\rm e}^{4r}\cosh 4g[(2-2L+3L^2)\cosh 4r - L^2] \\
& - 2{\rm e}^{4r}(4-4L+3L^2), \\
\Delta_2 =\ & {\rm e}^{4r}L^2[(1-L)^2\cosh 4g + 2(2-2L+L^2)\cosh^2 2r] \\
& + {\rm e}^{4r}(2-4L+3L^2-2L^3+L^4) \\
& + 2{\rm e}^{2r}\left(1+{\rm e}^{4r}\right)(1-L)L\left(1-L+L^2\right)\cosh 2g.
\end{aligned} \tag{38}$$

In Figs. 2 and 3 we give the QFI against lossy rate to intuitively show the precision bound in the presence of photon loss. It turns out that the precision bound is inferior to the Heisenberg limit even for a small lossy rate. As the lossy rate increases, the precision bound gradually degrades to the shot-noise limit. For a fixed g, the degradation of precision bound slightly slows down with the decrease of r, as shown in Fig. 2. Figure 3 shows that, for a fixed r, the precision bound degrades to the shot-noise limit with a slightly faster pace with the decrease of g. This may be due to the fact that, for a fixed r, the correlation between the two modes can be improved with increasing g. On the whole, it is beneficial for improving the tolerance against photon loss by reducing the proportion of photon number of the inputs when the total number of photons is fixed.

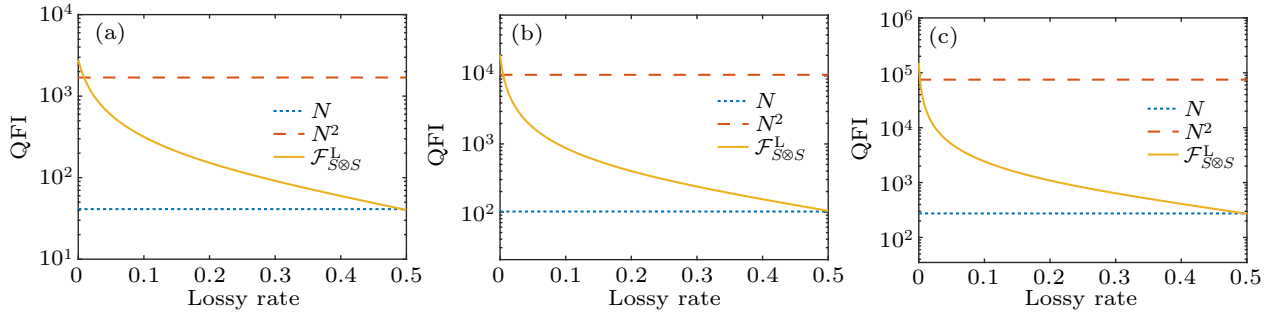


Fig. 2. The QFI in the presence of photon loss as function of lossy rate with $g = 2$: (a) $r = 0.5$, (b) $r = 1$, (c) $r = 1.5$.

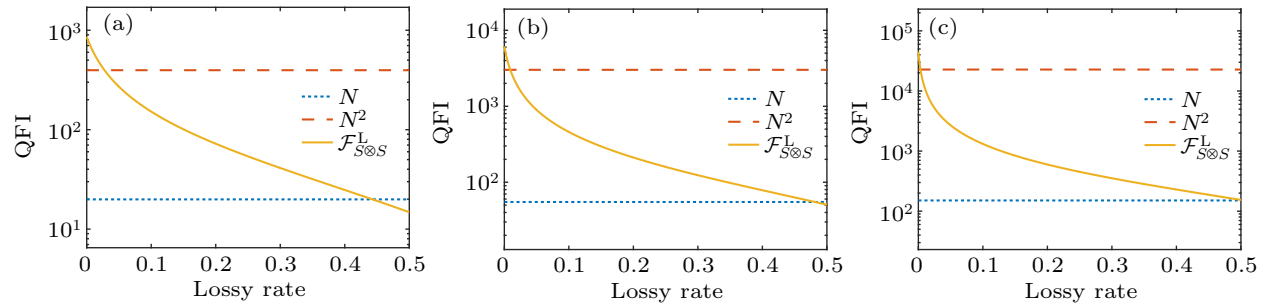


Fig. 3. The QFI in the presence of photon loss as a function of lossy rate with $r = 1.2$: (a) $g = 1$, (b) $g = 1.5$, (c) $g = 2$.

In general, pure quantum schemes are sensitive to photon loss. Here we compare the precision bound of our (pure quantum) scheme with that of the (classical-quantum hybrid) scheme using coherent along with squeezed vacuum states (see Appendix for detailed calculation). Let us consider quantum advantage, which is defined as

$$\mathcal{A}_{\rm Q}=\frac{\mathcal{F}^{\rm L}_{S\otimes S}}{\mathcal{F}^{\rm L}_{C\otimes S}}-1. \tag{39}$$

The positive and negative values indicate that a pure quantum scheme is superior and inferior to a classical-quantum hybrid scheme, respectively.

Figure 4 gives the dependence of quantum advantage on the lossy rate. The advantage of the pure quantum scheme is remarkable for an extremely low L, but this advantage gradually disappears with the increase of L. This suggests that, when compared with the classical-quantum hybrid scheme, the pure quantum scheme has superior precision in the absence of photon loss, but its robustness to loss is slightly inferior. Here we denote the lossy rate corresponding to $\mathcal{A}_{\rm Q}=0$ as $L_{\max}$ (marked points with values), and then $[0, L_{\max}]$ is called the range of quantum advantage. For $L>L_{\max}$, quantum advantage completely disappears and the classical-quantum hybrid scheme becomes an optimal candidate. It can be seen from the figure that the range of quantum advantage is larger for a large g or a low r.

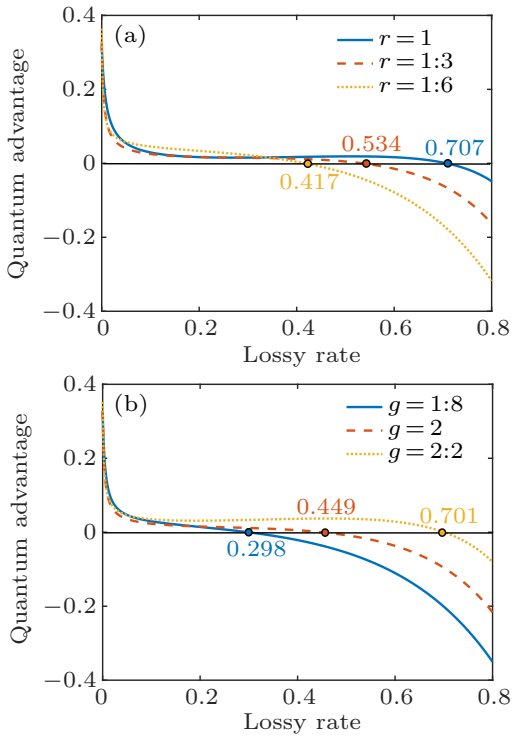


Fig. 4. The quantum advantage as a function of lossy rate with (a) $g=2$ and (b) $r=1.4$.

It should be noted that quantum advantage is not only related to L. For example, quantum advantage with $r=1.6$ is superior to that with $r=1$ for $L=0.2$ in Fig. 4(a), whereas opposite result is shown for $L=0.4$. Within the range of quantum advantage, as the increase of L, more significant quantum advantage can be obtained by decreasing r or increasing g. In fact, increasing g for a fixed r equals decreasing r for a fixed g. Both of which are beneficial for improving the robustness of scheme since the correlation between two modes is enhanced.

5. Conclusion

In summary, we addressed the problem of quantum phase estimation using two-mode squeezed Gaussian states. We analyzed the precision bound through the use of the quantum Fisher information. By maximizing the precision bound, two squeezed vacuum states were determined as the optimal inputs. For a lossless environment, the precision bound can scale as $N^{-1}/2$. In the presence of photon loss, sub-shot-noise-limited precision bound can be attainable with the lossy rate below 0.4. These results may be beneficial for practical quantum metrology based on nonlinear dynamics.

Appendix A: Transformation matrices of optical processes

Here we show the calculation method for the transformation matrices of the optical processes. Let us consider an OPA as an example. Based on operator relation in Eqs. (8) and (9), we have

$$\begin{aligned}&\hat{S}^{\dagger}_{\rm OPA}(\hat{a}^{\dagger}+\hat{a})\hat{S}_{\rm OPA}\\&=(\hat{a}^{\dagger}+\hat{a})\cosh g+(\mathrm{e}^{\mathrm{i}\phi}\hat{b}^{\dagger}+\mathrm{e}^{-\mathrm{i}\phi}\hat{b})\sinh g\\&=(\hat{a}^{\dagger}+\hat{a})\cosh g+(\hat{b}^{\dagger}+\hat{b})\sinh g\cos\phi\\&\quad+\mathrm{i}(\hat{b}^{\dagger}-\hat{b})\sinh g\sin\phi.\end{aligned}$$

Hence, the matrix elements in the first row are found to be $U_{\rm OPA,11}=\cosh g$, $U_{\rm OPA,12}=0$, $U_{\rm OPA,13}=\sinh g\cos\phi$, and $U_{\rm OPA,14}=\sinh g\sin\phi$, respectively. Further, we can determine all matrix elements of $\boldsymbol{U}_{\rm OPA}$, as shown in Eq. (14). Similarly, we can determine all matrix elements of $\boldsymbol{U}_{\rm PE}$ via the following operator relation:

$$\hat{U}^{\dagger}_{\rm PE}(\varphi)\hat{a}\hat{U}_{\rm PE}(\varphi)=\hat{a}\,\mathrm{e}^{-\mathrm{i}\varphi}, \tag{A1}$$

$$\hat{U}^{\dagger}_{\rm PE}(\varphi)\hat{b}\hat{U}_{\rm PE}(\varphi)=\hat{b} \tag{A2}$$

with $\hat{U}_{\rm PE}(\varphi)=\exp(-\mathrm{i}\hat{a}^{\dagger}\hat{a}\varphi)$ being the operator for phase encoding.

Appendix B: QFI of a lossy classical-quantum hybrid scheme

Here we give the QFI of a lossy scheme using coherent and squeezed vacuum states. We assume that the coherent and squeezed vacuum states are injected via modes a and b, respectively. The phase of displacement parameter and that of squeezing parameter are 0 and π, which are the optimal phase-matching condition. Accordingly, the mean vector of the inputs is given by

$$\boldsymbol{M}'_{\rm in}=[\ 2|\alpha|\quad 0\quad 0\quad 0\ ]^{\rm T}, \tag{B1}$$

and the covariance matrix of the inputs is given by

$$\boldsymbol{\Sigma}'_{\rm in} = \begin{bmatrix} 1 & 0 & 0 & 0 \\ 0 & 1 & 0 & 0 \\ 0 & 0 & \mathrm{e}^{2r} & 0 \\ 0 & 0 & 0 & \mathrm{e}^{-2r} \end{bmatrix}. \tag{B2}$$

Based on the method in the main text, the QFI takes the form

$$\mathcal{F}^{\rm L}_{C\otimes S} = \frac{1-L}{4}\left[\frac{\gamma_1}{\gamma_2} + \frac{\gamma_3}{\gamma_4}\right] \tag{B3}$$

with

$$\begin{aligned}\gamma_1 =& 4(1-L)\cosh^2 r\sinh^2 2g[L^2 + \mathrm{e}^{4r}L^2 + 2\mathrm{e}^{2r}(2-2L+L^2) \\ &+ (1+\mathrm{e}^{2r})^2(1-L)L\cosh 2g] \\ &- 4(1-L)\cosh^2 r\sinh^2 g\{\mathrm{e}^{4r}(8-17L+15L^2) \\ &- \mathrm{e}^{2r}(24-38L+34L^2) - (1+\mathrm{e}^{2r})^2(1-L)L\cosh 4g \\ &+ 8 - 17L + 15L^2 - 2\cosh 2g[4-7L+8L^2 \\ &+ \mathrm{e}^{4r}(4-7L+8L^2) - 2\mathrm{e}^{2r}(2-7L+8L^2)]\}, \end{aligned} \tag{B4}$$

$$\begin{aligned}\gamma_2 =& (1+\mathrm{e}^{2r})^2[4L(1-2L+2L^2-L^3)\cosh 2g \\ &+ (1-L)^2L^2\cosh 4g] \\ &+ \mathrm{e}^{2r}(8-16L+18L^2-12L^3+6L^4) \\ &+ (1+\mathrm{e}^{4r})(5L^2-6L^3+3L^4), \end{aligned} \tag{B5}$$

$$\begin{aligned}\gamma_3 =& 8|\alpha|^2\cosh^2 g[1-\mathrm{e}^{2r}(1-3L) - L \\ &+ (1+\mathrm{e}^{2r})(1-L)\cosh 2g], \end{aligned} \tag{B6}$$

$$\gamma_4 = 1 - 2L + \left(1+\mathrm{e}^{2r}\right)L^2 + \left(1+\mathrm{e}^{2r}\right)(1-L)L\cosh 2g. \tag{B7}$$

Acknowledgements

Project supported by the National Natural Science Foundation of China (Grant No. 12104193) and the Program of Zhongwu Young Innovative Talents of Jiangsu University of Technology (Grant No. 20230013).

References

[1] Braunstein S L and Caves C M 1994 *Phys. Rev. Lett.* **72** 3439
[2] Liu J, Yuan H, Lu X M and Wang X 2019 *J. Phys. A: Math. Theor.* **53** 023001
[3] Anisimov P M, Raterman G M, Chiruvelli A, Plick W N, Huver S D, Lee H and Dowling J P 2010 *Phys. Rev. Lett.* **104** 103602
[4] Nielsen J A H, Neergaard-Nielsen J S, Gehring T and Andersen U L 2023 *Phys. Rev. Lett.* **130** 123603
[5] Qin J, Deng Y H, Zhong H S, Peng L C, Su H, Luo Y H, Xu J M, Wu D, Gong S Q, Liu H L, Wang H, Chen M C, Li L, Liu N L, Lu C Y and Pan J W 2023 *Phys. Rev. Lett.* **130** 070801
[6] Guo Y F, Zhong W, Zhou L and Sheng Y B 2022 *Phys. Rev. A* **105** 032609
[7] Dowling J P 2008 *Contemp. Phys.* **49** 125
[8] Israel Y, Rosen S and Silberberg Y 2014 *Phys. Rev. Lett.* **112** 103604
[9] Joo J, Munro W J and Spiller T P 2011 *Phys. Rev. Lett.* **107** 083601
[10] Lee S Y, Ihn Y S and Kim Z 2020 *Phys. Rev. A* **101** 012332
[11] Pezzé L and Smerzi A 2008 *Phys. Rev. Lett.* **100** 073601
[12] Zhang J D and Wang S 2023 *Phys. Rev. A* **107** 043704
[13] Liu J, Shao T, Li C, Zhang M, Hu Y, Chen D and Wei D 2024 *Chin. Phys. B* **33** 014203
[14] Plick W N, Dowling J P and Agarwal G S 2010 *New J. Phys.* **12** 083014
[15] Chekhova M V and Ou Z Y 2016 *Adv. Opt. Photon.* **8** 104
[16] Ou Z Y and Li X 2020 *APL Photon.* **5** 080902
[17] You C, Adhikari S, Ma X, Sasaki M, Takeoka M and Dowling J P 2019 *Phys. Rev. A* **99** 042122
[18] Xu Y, Chang S, Liu C, Hu L and Liu S 2022 *Opt. Express* **30** 38178
[19] Chang S, Ye W, Zhang H, Hu L, Huang J and Liu S 2022 *Phys. Rev. A* **105** 033704
[20] Xu Y, Zhao T, Kang Q, Liu C, Hu L and Liu S 2023 *Opt. Express* **31** 8414
[21] Liu J, Shao T, Wang Y, Zhang M, Hu Y, Chen D and Wei D 2023 *Opt. Express* **31** 27735
[22] Liu M, Zhang L and Miao H 2023 *New J. Phys.* **25** 103051
[23] Wang S, Zhang J and Xu X 2022 *Opt. Commun.* **505** 127592
[24] Wong W C and Li J 2023 *New J. Phys.* **25** 033018
[25] Zuo X, Yan Z, Feng Y, Ma J, Jia X, Xie C and Peng K 2020 *Phys. Rev. Lett.* **124** 173602
[26] Du W, Kong J, Bao G, Yang P, Jia J, Ming S, Yuan C H, Chen J F, Ou Z Y, Mitchell M W and Zhang W 2022 *Phys. Rev. Lett.* **128** 033601
[27] Kong J, Ou Z Y and Zhang W 2013 *Phys. Rev. A* **87** 023825
[28] Zhang J D, Jin C F, Zhang Z J, Cen L Z, Hu J Y and Zhao Y 2018 *Opt. Express* **26** 33080
[29] Zhang J D, You C, Li C and Wang S 2021 *Phys. Rev. A* **103** 032617
[30] Lang M D and Caves C M 2013 *Phys. Rev. Lett.* **111** 173601
[31] Zhang J D, You C and Wang S 2022 *Opt. Express* **30** 43143
[32] Sparaciari C, Olivares S and Paris M G A 2015 *J. Opt. Soc. Am. B* **32** 1354
[33] Weedbrook C, Pirandola S, García-Patrón R, Cerf N J, Ralph T C, Shapiro J H and Lloyd S 2012 *Rev. Mod. Phys.* **84** 621
[34] Monras A and Paris M G A 2007 *Phys. Rev. Lett.* **98** 160401
[35] Li D, Gard B T, Gao Y, Yuan C H, Zhang W, Lee H and Dowling J P 2016 *Phys. Rev. A* **94** 063840
[36] Gao Y and Lee H 2014 *Eur. Phys. J. D* **68** 347
[37] Agafonov I N, Chekhova M V and Leuchs G 2010 *Phys. Rev. A* **82** 011801
[38] Zhang J D and Wang S 2023 *Chin. Phys. B* **32** 010306
[39] Sparaciari C, Olivares S and Paris M G A 2016 *Phys. Rev. A* **93** 023810
[40] Ono T and Hofmann H F 2010 *Phys. Rev. A* **81** 033819
[41] Gard B T, You C, Mishra D K, Singh R, Lee H, Corbitt T R and Dowling J P 2017 *EPJ Quantum Technol.* **4** 4